







Identification of the mechanism responsible for the boron oxygen light induced degradation in silicon photovoltaic cells

Cite as: J. Appl. Phys. **125**, 185704 (2019); doi: [10.1063/1.5091759](https://doi.org/10.1063/1.5091759)

Submitted: 5 February 2019 · Accepted: 24 April 2019 ·

Published Online: 14 May 2019



Michelle Vaqueiro-Contreras,^{1,a)}  Vladimir P. Markevich,^{1,b)}  José Coutinho,²  Paulo Santos,²  Iain F. Crowe,¹  Matthew P. Halsall,¹  Ian Hawkins,¹ Stanislav B. Lastovskii,³ Leonid I. Murin,³ and Anthony R. Peaker^{1,b)} 

AFFILIATIONS

¹Photon Science Institute, School of Electrical and Electronic Engineering, The University of Manchester, Manchester M13 9PL, United Kingdom

²Department of Physics and I3N, University of Aveiro, Campus Santiago, 3810-193 Aveiro, Portugal

³Scientific-Practical Materials Research Center of the National Academy of Sciences of Belarus, Minsk 220072, Belarus

^{a)}**Present address:** Photovoltaic & Renewable Energy Engineering, Tyree Energy Technologies Building, University of New South Wales, Sydney NSW 2052, Australia

^{b)}**Authors to whom correspondence should be addressed:** v.markevich@manchester.ac.uk; a.peakier@manchester.ac.uk

ABSTRACT

Silicon solar cells containing boron and oxygen are one of the most rapidly growing forms of electricity generation. However, they suffer from significant degradation during the initial stages of use. This problem has been studied for 40 years resulting in over 250 research publications. Despite this, there is no consensus regarding the microscopic nature of the defect reactions responsible. In this paper, we present compelling evidence of the mechanism of degradation. We observe, using deep level transient spectroscopy and photoluminescence, under the action of light or injected carriers, the conversion of a deep boron-di-oxygen-related donor state into a shallow acceptor which correlates with the change in the lifetime of minority carriers in the silicon. Using *ab initio* modeling, we propose structures of the B_3O_2 defect which match the experimental findings. We put forward the hypothesis that the dominant recombination process associated with the degradation is trap-assisted Auger recombination. This assignment is supported by the observation of above bandgap luminescence due to hot carriers resulting from the Auger process.

© 2019 Author(s). All article content, except where otherwise noted, is licensed under a Creative Commons Attribution (CC BY) license (<http://creativecommons.org/licenses/by/4.0/>). <https://doi.org/10.1063/1.5091759>

I. INTRODUCTION

Silicon photovoltaics dominate the solar cell market and will soon provide one of the lowest cost options for future electricity supply. The last decade has seen prices fall and efficiencies increase, resulting in near exponential growth in silicon solar installations.¹ However, it has been known for over 40 years that solar cells with the active region made from boron-doped silicon and containing oxygen (the most common configuration) degrade significantly during the first few hours of operation at ambient temperatures. The degradation process is commonly called light-induced degradation (LID), and the resultant condition of the cell is referred to as the “degraded state.”

A substantial published literature now exists on this topic (>250 papers reporting research and >1000 referring to the effect),

with the primary diagnostic research tool being minority carrier lifetime measurements subsequently related to cell performance. The available results and current understanding of the problem have been reviewed recently by Niewelt *et al.*²

It has been found that, in general, the LID occurs in two stages. These are (i) a fast process which occurs on the time scale of seconds and has a relatively weak temperature dependence and (ii) an asymptotic process with a time scale of tens of hours with an activation energy of formation of the degradation-related defects of about 0.48 eV.^{2,3} The relation between the defects formed at the fast and slow stages of degradation is debatable: it is argued that they are either independent or can be transformed to each other.^{2–4} The degradation during the slow process is usually much more

severe than that during the fast process, so the defects formed at the slow stage are thought to be responsible for the change in the efficiency of solar cells from boron and oxygen doped silicon upon light soaking. In this work, we concentrate on the defects that are formed during the slow stage of LID.

Although there are significant variations in the published data, there is a consensus that concentration of defects responsible for the light-induced degradation depends on the square of the oxygen concentration and increases almost linearly with the boron concentration in uncompensated B-doped silicon.^{2,3} The presence of boron is also necessary for the occurrence of LID in compensated p- and n-type silicons; however, in the compensated materials, the data on dependencies of concentration of recombination active defects vs boron concentration or majority carrier concentration are controversial and debatable.² The light-induced degradation does not occur if the acceptor is gallium instead of boron.

Although the process is generally referred to as LID, it has been shown that at the heart of the degradation mechanism is the presence of minority carriers (electrons) which appear as a result of the above bandgap illumination. Experiments with carrier injection from a p-n junction produce an identical form of degradation sometimes labeled as carrier induced degradation (CID).⁵ As there are other light induced degradation processes unrelated to that discussed above,⁶ we will refer to the boron oxygen process as “BO degradation.”

The recombination process can be deactivated by annealing at around 200 °C for several minutes in the dark, the defect so being converted into what is referred to as the “annealed state.”^{2,3} However, on subsequent exposure to light, degradation occurs again. This degradation cycle can be eliminated by annealing at elevated temperatures under illumination so forming what is referred to as the “stabilized state.”^{2,7} Unfortunately, this “stabilized” state is also metastable and can be returned to the annealed state by dark annealing at ~200 °C for ~100 min. The cycles are illustrated in Fig. 1.

The magnitude of the degradation in high quality commercial devices can be up to 10% relative, i.e., ~2% absolute. It occurs in single crystal Czochralski (Cz) grown silicon and to a lower extent in multicrystalline cast silicon because of lower oxygen concentration in this material.⁸ The greatest effects occur in those devices

with higher efficiencies and have been reported to be particularly marked in advanced cell structures currently being implemented by the solar industry such as PERC (passivated emitter rear cell) designs. A number of methodologies have been developed to reduce LID involving heat treatments or passivation with hydrogen. These have been reviewed recently by Hallam *et al.*,⁹ but a key question is whether such treatments will ensure stability during the 25 year working life of a solar cell. As a consequence, a more complete understanding of the degradation mechanism is of considerable commercial importance. Despite the vast literature on this topic, the microscopic structures of the three states and mechanisms of transformations between them are not known,² and it is this issue that we address in this paper.

Many studies of minority carrier lifetime degradation are mostly interpreted as resulting from a Shockley–Read–Hall (SRH) recombination center in the bandgap. The properties of the implied SRH center have been derived from temperature-dependent lifetime spectroscopy (TDLS) and injection-dependent lifetime spectroscopy (IDLS). Schmidt and Cuevas obtained values of energy level position of the recombination active BO center between $E_V+0.35$ eV and $E_C-0.45$ eV using these techniques.¹⁰ Rein and Glunz refined these measurements and placed the energy level at $E_C-0.41$ eV using a detailed SRH analysis of the TDLS behavior.¹¹ This revealed that the recombination center behaves as an attractive Coulombic center for electrons with an electron capture cross section σ_n exhibiting a T^{-2} dependency and a ratio of electron to hole capture cross sections $\sigma_n/\sigma_p = 9.3$. It has been argued recently that the degradation induced recombination center is a defect with negative- U properties having a donor level at about $E_C-0.41$ eV and an acceptor level at about $E_V+0.26$ eV.^{2,4,12,13} The ratio of electron to hole capture cross sections for the donor level has been observed to be in the range between 10 and 20.^{12,13} Assuming physically feasible maximum values for σ_n and the observed lifetime changes, observation of the responsible SRH center using standard techniques, such as deep level transient spectroscopy (DLTS) and its minority carrier equivalent (MCTS), should present no difficulty.^{14,15}

However, although several species of deep level defects have been observed in the degraded Cz-Si:B material, no one has detected SRH states with directly measured minority carrier cross sections and concentrations which could account for the observed lifetime reduction or which scale with the BO degradation. In 2015, Mchedlidze and Weber detected deep states in DLTS spectra of BO-degraded material which were not present in undegraded Cz-Si:B material or in Ga-doped Si which had been exposed to light.¹⁶ These states disappeared after 200 °C annealing in line with BO degradation. In consequence, Mchedlidze and Weber have proposed that these states at $E_C-0.41$ eV and $E_V+0.37$ eV are the SRH centers responsible for BO degradation.¹⁶ They used diodes fabricated from PERC solar cells and put forward the hypothesis that previous attempts to observe the BO-related states were unsuccessful because of hydrogen contamination passivating the electrically active defects when Schottky diodes were fabricated for characterization.

Our earlier work on transition metal defects supports the hypothesis that classic fabrication methods of Schottky barrier diodes on silicon introduce hydrogen and can passivate recombination centers.¹⁷ In further support of this passivation concept, Hallam *et al.* have studied hydrogenation as a means of eliminating

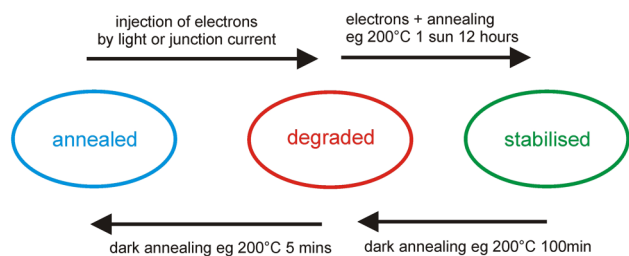


FIG. 1. Block diagram of the BO LID-related defect states and processes. Overview of the ground and two metastable states of the BO-related defect according to the results reported in the literature and using the nomenclature of Niewelt *et al.*²

BO degradation.¹⁸ In the present work, we have fabricated n^+-p diodes from Si material without hydrogen involvement. In these structures, we have observed BO degradation using measurements of minority carrier lifetime in the finished diodes. However, we have not detected the states observed by Mchedlidze and Weber.

In contrast, in this paper, we observe a DLTS peak due to a deep trapping center with an activation energy for hole emission of 0.97 eV present in the undegraded material. After minority carrier (electron) injection, which results in BO degradation, the trapping center decreases in concentration. The reduction of the trapping center concentration correlates strongly with a decrease in minority carrier lifetime and an increase in the majority carrier (hole) concentration, p . Furthermore, from admittance spectroscopy and photoluminescence (PL) measurements of the degraded samples, we have found that the increase in p is associated with the appearance of a shallow acceptor. In low-temperature PL, this is observed as a bound exciton (BE) line that is close to that due to B_s atoms and is not present in the undegraded material. The disappearance of the observed DLTS peak associated with the deep donor has been directly correlated with lifetime degradation in the Si diodes upon carrier injection and its reappearance upon thermal treatments with the material's lifetime recovery, thus following the behavior pattern of the much reported BO degradation. From the analysis of the capture and emission kinetics of holes by the defect, its configuration coordinate (CC) diagram has been constructed. It is argued that capture and emission of charge carriers by the defect result in changes in the atomic configurations of the complex. *Ab initio* calculations indicate that the electronic properties of the defect consisting of one substitutional boron atom and two interstitial oxygen atoms (B_sO_2) are very different in different atomic configurations. Depending on the position of the Fermi level (E_F), the defect either can be a deep donor or it can be in one of two configurations with shallow acceptor levels. The model is consistent with the DLTS and PL measurements, and besides showing transformation barriers compatible with the degradation/recovery kinetics of the cells, it also accounts for the resilience of Ga-doped material to LID. It is suggested the BO degradation of minority carrier lifetime in solar cells containing boron and oxygen is associated with trap-assisted Auger recombination of charge carriers through the B_sO_2 complex, which, in its recombination active state, is a shallow acceptor.

II. EXPERIMENTAL AND THEORETICAL METHODS

A. Experimental details

1. Samples

We have used n^+-p-p^+ and Schottky barrier diodes on p -type Czochralski-grown Si materials to study the boron–oxygen defects. The diodes were formed by implantation and subsequent thermal activation of 60 keV phosphorus ions (front side) and 60 keV boron ions (back side) in boron-doped commercial electronic grade Cz-Si wafers with a resistivity of 3 and 10 Ω cm. The diode area was 4.4 and 6.25 mm² for the 3 and 10 Ω cm materials, respectively, and a leakage current at 10 V reverse bias was $\sim 10^{-6}$ A. The concentration of interstitial oxygen [O_i] in the diodes from 3 and 10 Ω cm materials was estimated as $(7.5 \pm 1) \times 10^{17}$ cm⁻³ and $(9.5 \pm 1) \times 10^{17}$ cm⁻³, respectively, from the rates of capture of

interstitial carbon atoms by the O_i atoms determined from annealing experiments on some of the diodes irradiated with alpha particles at 260 K.^{19,20} Schottky barrier diodes (1 mm in diameter) were prepared by thermal evaporation of a titanium/aluminum stack through a shadow mask on samples from a few p -type Cz-Si crystals with initial resistivity from 1 to 10 Ω cm. Concentrations of interstitial oxygen (O_i) and substitutional carbon (C_s) atoms in these crystals have been determined from magnitudes of infrared absorption lines at 1107 and 605 cm⁻¹ in the spectra measured at room temperature. Calibration coefficients of 3.14×10^{17} cm⁻² and 0.94×10^{17} cm⁻² have been used for the O_i and C_s atoms, respectively. The oxygen concentration in the crystals was in the range from 7×10^{17} cm⁻³ to 1×10^{18} cm⁻³, and the carbon concentration was below 2×10^{16} cm⁻³. Some of the samples have been treated in the temperature range from 350 to 425 °C to generate boron–oxygen-related defects. The heat treatments resulted in decreases in the noncompensated shallow acceptor concentration and, therefore, in the capacitance of the diodes, but did not result in significant changes of their leakage current and ideality factor.

2. Junction capacitance measurements

Current–voltage and capacitance–voltage (C – V) measurements have been carried out in order to evaluate the quality of the diodes and to determine the uncompensated shallow acceptor concentration and width of the probed depletion regions. Deep level transient spectroscopy and high-resolution Laplace DLTS (L-DLTS) techniques²¹ have been used for the detection of carrier emission from deep defect states. Measurements of changes in total capacitance of the diodes resulted from filling the depletion regions with holes have been used to monitor transformations of the B–O defects from the shallow acceptor state to the deep donor state. Admittance spectroscopy measurements have been used for the detection of shallow level acceptors in the diodes as described in the [supplementary material](#).

3. Minority carrier lifetime measurements

Two techniques were used for the carrier lifetime measurements dependent on whether the samples were wafers or diodes. In the case of wafers, the microwave photoconductance decay technique was used to map the lifetime across the slices of silicon used. This was done with an industry standard Semilab WT-2000PVN instrument incorporating 905 nm laser excitation, a laser bias source, and conductivity decay measurements with an ~ 10 GHz microwave source. The lifetime measurements represent an averaged lifetime in the sample at a depth of a few tens of micrometers from the surface. For suppression of surface recombination, the maps were recorded after a dip in diluted hydrofluoric acid with both surfaces of the samples covered with iodine/ethanol solution during the measurement.

In the case of the diodes, the minority carrier lifetime was measured with the reverse recovery method.²² This technique, which is widely used in the power semiconductor industry, measures the reverse current in the diode as a function of time after application of a forward bias pulse and the potential applied to the diode is switched to zero. The excess minority carrier density generated during forward bias creates a reverse current which sweeps out the carriers. From the current response, two key phases can be distinguished: the storage phase and the recovery phase, which can be

represented by an exponential function. The storage time which is often well defined can then be related to the effective minority carrier lifetime. The analysis is described in detail by Kuno²² and is reproduced in many standard texts. In our n^+p - p^+ diodes, the technique gives the lifetime of electrons in the p -type region. The technique tends to underestimate the lifetime because of recombination in the n^+ region and surface recombination. However, in the context which we have used it, this is an excellent measure of relative lifetime.

4. Low-temperature photoluminescence measurements

Two samples were studied by low-temperature PL. These were cut from the same slice of Cz-Si:B, both annealed at 700 °C + 400 °C and only one subsequently exposed to 1 sun illumination for 60 h at 40 °C. The samples were mounted in close proximity on a 1 in. diameter copper disk, using silver DAG (a suspension of fine flake silver in methyl isobutylketone) as a thermal bond. The disk containing the samples was mounted on the cold finger of a recycling helium cryostat and kept under vacuum (10^{-6} mbar) for 24 h before performing measurements. Photo-excitation was provided by a 780 nm SacherLasertechnik diode laser (penetration depth in Si is several micrometers) with a spot size (on the sample) of approximately 2 mm and a laser power (measured at the cryostat entrance window) of 1.5 mW. The PL signal was collimated and focused on the entrance slit of a Horiba iHR550 spectrometer, in which it was dispersed using a 600 g/mm grating and detected using a liquid nitrogen cooled InGaAs array. The spectra were integrated for 10 s with the result derived from the average of three accumulations. The sample temperature was recorded using a thermocouple mounted to the rear of the cold finger as close as possible to the sample position and read using an Oxford ITC4 temperature controller. Measurements were made for both samples in brief succession after the recorded sample temperature (11 K) had been stable for several hours. No difference in the recorded sample temperature was noted with the laser on and off. In order to maximize signal-to-noise for the highest resolution measurements, the most intense peaks, corresponding to the TO (transverse optical) phonon assisted PL band, were recorded. The energy of the TO replica of a bound exciton (BE) is

$$E_{\text{BE} - \text{TO}}^{(\text{B})} = E_{\text{g}} - E_{\text{FE}} - E_{\text{TO}} - E_{\text{BE}}^{(\text{B})},$$

where E_{FE} is the energy of the free exciton, E_{TO} is the TO phonon energy, and $E_{\text{BE}}^{(\text{B})}$ is the binding energy of the exciton to the neutral boron atom. This latter energy is dependent on the chemical nature of the dopant (central cell correction) and is described by an empirical relationship known as Haynes' rule,²³ which relates the exciton binding energy to the ionization energy (E_{i}) of the dopant. For the case of boron: $E_{\text{i}}^{(\text{B})} = 45$ meV and $E_{\text{BE}} \sim 0.1 \times E_{\text{i}}$ (Haynes' rule) $\rightarrow E_{\text{BE}}^{(\text{B})} \sim 4.5$ meV. It is this relationship which is used to calculate the hole ionization energy for the defect associated with the BO degradation.

5. Photon counting photoluminescence (Auger electrons)

Above gap luminescence was detected using a bespoke micro-photoluminescence system. The system was described elsewhere²⁴ for measurements of InGaN photoluminescence and was adapted

for the measurement described above by automated control of the "probe" laser. The sample is excited with 10 mW from a fiber coupled 980 nm laser focused to a large laser spot around 100 μm in diameter incident at 45° to the sample surface. The PL is collected by a long working distance microscope objective with a numerical aperture of 0.4, passed through a short pass filter to remove any residual laser light and collimated into a large core optical fiber for measurement by a spectrometer equipped with a volume phase holographic diffraction grating and a cooled CCD detector, giving a >80% detection probability for every collected photon. To observe the weak above gap light, it is necessary to measure photon count rates of <0.1 photons/s. This is challenging experimentally, with small drifts in temperature of the detector causing the dark count to vary more than this. To achieve the necessary sensitivity, the laser was switched on and off by a 0.1 Hz square wave signal, 400–1000 consecutive 5 s exposures were then taken, triggered by either the rising or falling edge of the square wave and recorded. The final spectrum was obtained by adding alternate spectra and subtracting the "on" spectra from the "off" ones. The resulting spectra were further smoothed by a running average of 10 pixels across the spectrum. This resulted in a noise level of around 0.02 photons/s. Spectra are corrected for the response of the detector and spectrometer. The choice of exposure (chopping rate) was a compromise between readout noise, dark noise, and thermal drift in the detector. 5 s exposure on the detector gives a dark noise of roughly 5 photons, which is equivalent to several times the read out noise. Longer exposures caused thermal drifts to be significant due to the time between laser off and laser on exposures increasing the effect of any thermal drift. In the previous work by Hangleiter²⁵ on hot luminescence due to trap Auger recombination in silicon, a lower efficiency detection system was employed in the sense that a nonmicroscope system was used with a conventional spectrometer in combination with single channel detection using a photomultiplier tube. Each of these choices is less efficient than those used in our work, and the net effect is to reduce the exposure times from roughly one day for each spectral point in Hangleiter's case to a few hours across the spectra recorded by us.

B. Ab initio calculations

First-principles calculations were carried out within spin-polarized density functional theory, combining the projector-augmented wave (PAW) method and plane-waves to describe core and valence electronic states, respectively.^{26,27} Defect structures and transformation/migration mechanisms were investigated by considering the generalized gradient approximation to the many-body exchange-correlation potential.²⁸

Total energies of stable and transition-state structures obtained from semilocal calculations were refined by switching to the hybrid density functional of Heyd, Scuseria, and Ernzerhof (HSE).²⁹ This functional brings a portion of short-range exact exchange into the potential, leaving the long-range interactions to be treated within the simpler semilocal approximation. The range separation parameter was set to $\omega = 0.5 \text{ \AA}^{-1}$. By this approach, the quasiparticle gap, $E_{\text{g}}^{\text{QP}} = E(+) + E(-) - 2E(0)$, obtained from total energies $E(q)$ of charged (bulk) supercells was 1.15 eV, essentially matching an experimental value of 1.17 eV.

Construction of the PAW potentials assumed the following valence occupancy Si: $3s^2 3p^2$, B: $2s^2 2p^1$, and O: $2s^2 2p^4$. The kinetic energy cutoff for the plane-wave basis used was $E_{\text{cut}} = 400$ eV. Defects were incorporated into 216-atom cubic supercells made from $3 \times 3 \times 3$ conventional cells of Si. The HSE-level lattice parameter for bulk Si was $a_0 = 5.4318$ Å. The electron density and potential terms were calculated by sampling the band structure over a $2 \times 2 \times 2$ grid of k-points.³⁰ The convergence tolerance for the self-consistent energies was 10^{-7} eV, and forces for relaxed structures were lower than 10 meV/Å. The above conditions confer to the calculations a numerical accuracy of about 5 meV to energy differences like formation energies, binding energies, or ionization energies.

Electronic transitions of defects were obtained from ionization energies or electron affinities of defective supercells with respect to the energy of the valence band top. Total energies of charged supercells are affected by artificial Coulomb interactions due to periodic boundary conditions.³¹ For the case of deep states, these effects were mitigated by adding a charge correction to the energy as proposed by Freysoldt, Neugebauer, and Van de Walle.³² Such corrections were in the range 0.05–0.49 eV.

Minimum energy paths between stable structures were explored with the help of the nudged elastic band (NEB) method.³³ The NEB method optimizes a number of intermediate images (11 in the present study) along a reaction/transformation/migration path. During the optimization, neighboring images are connected through spring forces, enforcing equal spacing between them. Subsequently, we applied the climbing image NEB (CI-NEB) in which the highest energy NEB image is driven up along the energy surface to find the saddle point structure.

III. EXPERIMENTAL RESULTS

A. Detection of a precursor of the LID defect and evidence of the precursor \Leftrightarrow LID defect transformations

In the DLTS spectra recorded in the temperature range 300–440 K for nearly all of our as-manufactured diodes (both n - p junctions and Schottky diodes) from boron-doped Cz-Si, a previously unreported broad peak has been detected, with maximum at about 390 K (for emission rate window, $e_{\text{em}} = 10$ s⁻¹ and filling pulse length, $t_p = 100$ ms) [Fig. 2(a)]. We will refer to the

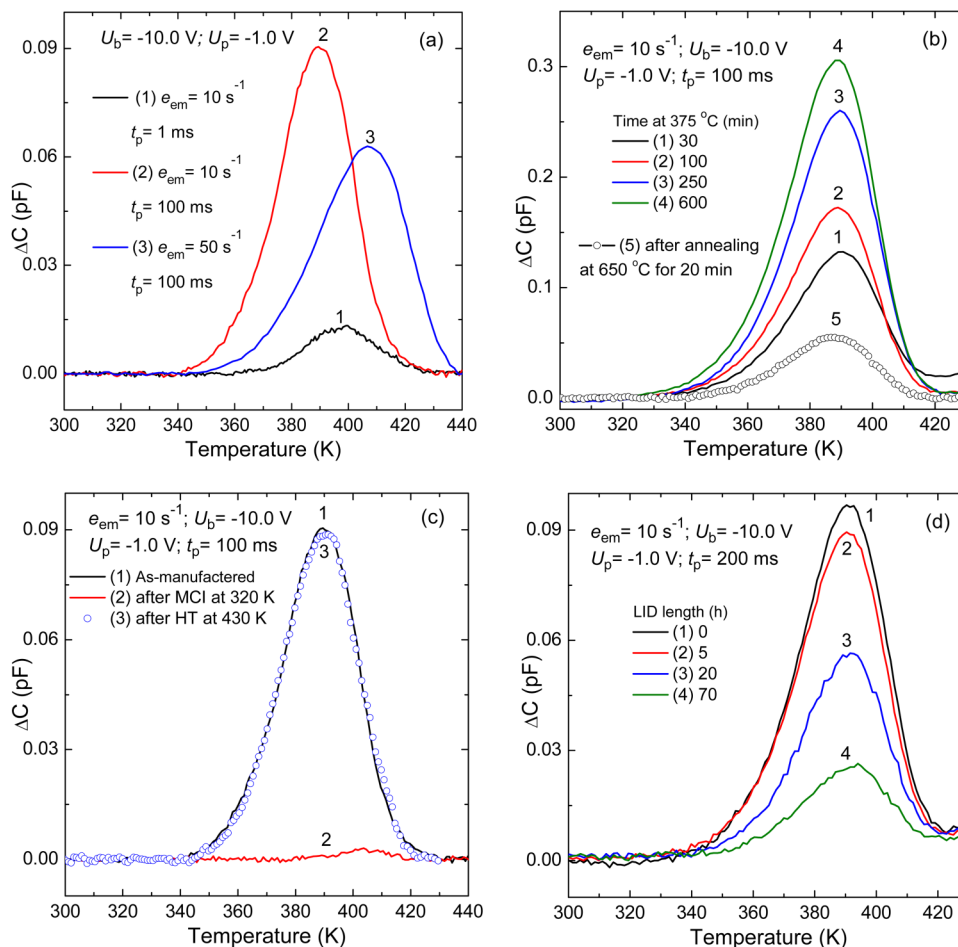


FIG. 2. Conventional DLTS spectra recorded in the temperature range 300–440 K on n^+p - p^+ diodes from 3 Ω cm p-type boron-doped Cz-Si material. (a) DLTS spectra recorded with different measurement conditions on an as-manufactured n^+p - p^+ diode. (b) DLTS spectra recorded on the n^+p - p^+ diodes, which were subjected to (1)–(4) heat treatments (HTs) of different durations (given in the graph) at 375 °C and (5) a heat treatment at 650 °C for 20 min followed by cooling down to room temperature at a rate of about 100 K/min. (c) DLTS spectra recorded on an n^+p - p^+ diode after the following sequential treatments: (1) as-manufactured, (2) forward bias (+2.5 V) induced injection of minority carriers (MCI) for 60 h at 320 K, and (3) annealing in the dark at 430 K for 100 min with no bias applied. (d) DLTS spectra recorded on an n^+p - p^+ diode after its illumination with light (of about 1 sun intensity) from a halogen lamp at room temperature. Measurement conditions for all the spectra are given in the figures.

corresponding emission signal as related to the H_{390} trap in the following discussion. The magnitude of the observed peak depends significantly on the t_p value [Fig. 2(a)]. Detection of the peak requires long filling pulses ~ 100 ms. These are unusual detection conditions for Si defects in terms of both the high temperature and the long filling pulse required, which are outside the typical experimental conditions employed for surveying traps in Si with DLTS. Also, the magnitude of the peak decreases with an increase in emission rate window, so indicating a smaller population of the corresponding trap with majority carriers (holes) with increasing temperature [Fig. 2(a)]. The concentration of the H_{390} trap varies in the range 5×10^{11} – 5×10^{12} cm^{-3} in the as-manufactured diodes from different Cz-Si:B materials.

It has been observed that the magnitude of the DLTS peak due to the H_{390} trap can be increased significantly upon annealing of the Cz-Si:B samples in the temperature range 350–450 °C and decreased upon annealing at temperatures exceeding 600 °C. Figure 2(b) shows changes in the magnitude of the peak in n^+p - p^+ diodes from 3 Ω cm Cz-Si:B material resulting from heat treatments at 375 °C and 650 °C.

Importantly, we have observed that the H_{390} trap disappears upon minority carrier injection (MCI) by either illumination or forward biasing of n^+p - p^+ diodes for relatively long periods of time (hours) at ambient temperatures and reappears upon heat treatments in the dark for $T > 130$ °C. Figure 2(c) shows the DLTS spectra for an n^+p - p^+ diode from the 3 Ω cm Cz-Si:B material, which was subjected to forward biasing for 60 h at 320 K inside the cryostat for DLTS measurements and subsequently annealed in the dark at 430 K for 100 min. It can be observed that the DLTS signal due to the H_{390} trap disappears after the MCI treatment and then

recovers after the annealing treatment in the dark. Such cycles of annihilation-recovery can be repeated indefinitely with negligible losses in the magnitude of the H_{390} trap. The DLTS spectra for a neighboring diode from the same wafer, which was subjected to illumination with a light intensity of about 1 sun for 5, 20, and 70 accumulated hours at room temperature, are shown in Fig. 2(d), revealing a clear decrease in magnitude of the H_{390} trap with increasing periods of light soaking.

We have carried out measurements of the effective minority carrier lifetime (τ_{eff}) in the n^+p diodes by means of the reverse recovery method²² and found a remarkable correlation between the disappearance and recovery of the H_{390} trap and the degradation and recovery of lifetime in the diodes studied. The data presented in Fig. 3 have been obtained from direct measurements of changes in τ_{eff} upon injection/annealing treatments in an n^+p - p^+ diode made from 3 Ω cm Cz-Si:B and annealed at 350 °C for 10 h and measurements of the changes in concentration of the H_{390} trap in the same sample. Figure 3(a) shows the normalized changes in reciprocal values of effective lifetime $\left[(1/\tau_{eff(i)} - 1/\tau_{eff(ann)}) / (1/\tau_{eff(degr)} - 1/\tau_{eff(ann)}) \right]$, which in the literature are often treated as relative changes in the effective concentration of the recombination active BO defect $\{[BO^*]\}$,^{2,3} and the normalized changes in concentration of the H_{390} trap resulting from the carrier injection treatment at 340 K. It can be observed that the decrease in the concentration of the H_{390} trap upon the injection treatment can be described by an exponential decay that occurred simultaneously with an exponential growth of $[BO^*]$. Figure 3(b), on the other hand, shows that the exponential increase in the H_{390} trap concentration upon subsequent dark annealing at 430 K occurred simultaneously with a decrease in $[BO^*]$. From the exponential fitting of the data

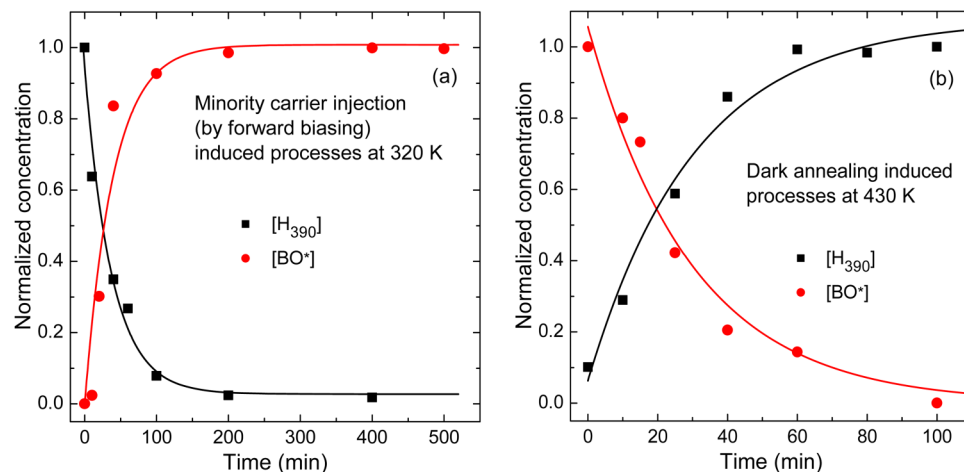


FIG. 3. Changes in normalized concentrations of the boron–oxygen-related defects in an n^+p - p^+ diode from 3 Ω cm p-type boron-doped CZ-Si material, which was annealed at 350 °C for 10 h. Changes in the normalized concentration of the H_{390} trap and the normalized effective concentration of the BO defect responsible for the lifetime degradation upon: (a) forward bias (+2.0 V) induced injection of minority carriers at 340 K and (b) annealing in the dark at 430 K with no bias applied. The concentration of the H_{390} trap has been determined from DLTS measurements and the effective concentration of the BO defect responsible for the lifetime degradation from reverse-recovery lifetime measurements on the same diode. The lifetime values were 26.3 μs in the annealed state and 21.9 μs in the degraded state, and the concentration of the H_{390} trap was $(9 \pm 1) \times 10^{12}$ cm^{-3} in the diode.

In the moderately doped p-type Si crystals, the H_{390} trap is in the positive charge state (state D^+ in Fig. 4) at room temperature. However, the charge state and configuration can be easily changed by short injection pulses of minority carriers (electrons) either by forward biasing of an n^+ -p diode or by the application of above bandgap light. Upon the minority carrier injection, the defect captures an electron and transforms to the A^- state according to the following sequence of reactions: $D^+ + h^+ + e^- \rightarrow X^0 + h^+ \rightarrow A^0 + h^+ \rightarrow A^- + 2h^+$. After the end of an injection pulse, the defect transforms back to the minimum energy D^+ configuration if holes are available and the temperature is high enough to surmount the large ΔE_{AX} energy barrier (Fig. 4). In n -p diodes, such injection pulses result in a sharp increase in bias capacitance C [which can be considered a measure of concentration of uncompensated shallow acceptors (or free holes) in the probed region] of the diodes studied with subsequent slow decays in C values upon the application of long filling pulses. It is worth mentioning that the H_{390} trap itself is not an effective recombination center as the capture and emission processes of both electrons and holes by the defect require surmounting the rather large energy barriers and are relatively slow.

As stated above, we have observed some traces of the H_{390} trap in all of our as-manufactured diodes (both n^+ -p and Schottky barrier types) on boron-doped Cz-Si crystals. The trap has not been detected in n^+ -p and Schottky barrier diodes fabricated from boron-doped float-zone Si crystals. Furthermore, we have tested a few Schottky barrier diodes on gallium-doped Cz-Si and have not detected the H_{390} trap or similar traps in Cz-Si:Ga. This is consistent with boron and oxygen atoms being incorporated into the defect responsible for the H_{390} trap. In the present study, we did not have access to a set of Si samples with a sufficiently wide range of measured oxygen and boron concentrations to obtain proper dependencies of the H_{390} trap concentration on $[O_i]$ and $[B_s]$. However, taking into account the evidence we have presented for the transformation of the H_{390} trap into the BO defect responsible for the light induced degradation (Fig. 3), and experimental data on the boron and oxygen concentration dependencies for the LID-BO center,^{2,3,34} we suggest that both defects contain one boron (substitutional) and two oxygen atoms (B_sO_2).

An important observation is that the concentration of the H_{390} trap can be increased significantly by the heat treatments of Cz-Si:B crystals in the temperature range 350–450 °C [Fig. 2(b)] and then reduced by heat treatments at temperatures exceeding 600 °C. These observations indicate that the B_sO_2 complex can be formed upon heat treatments in the temperature range where the oxygen dimer is mobile; however, the binding energy of the complex is not very high, so, heat treatments at $T \geq 600$ °C result in its dissociation. Unfortunately, the available literature results on effects of heat treatments in the temperature range 300–450 °C on lifetime LID in boron-doped Cz-Si crystals are not systematic and are controversial.² Multiple observations indicate that high-temperature (>600 °C) heat treatments of Cz-Si:B samples with fast cooling down after the treatments resulted in significant reductions of concentration of the boron-oxygen defect responsible for LID.^{2,35–37}

C. Electronic properties of the LID defect: Evidence for a shallow level center

The results presented above indicate that the BO-related LID is the result of transformation of the B_sO_2 defect from the configurations responsible for the H_{390} trap into another configuration in which the defect acts as an effective recombination center. The question now is what are the electronic properties of the B_sO_2 defect in this recombination active configuration? It is worth mentioning that the concentration of the H_{390} trap, which we have determined in some of the diodes subjected to heat treatments in the temperature range 350–450 °C, has been in excess of 10^{13} cm^{-3} . Deep level defects with concentrations higher than 10^{12} cm^{-3} can be easily detected in either DLTS or MCTS spectra.^{14,15} Despite this, and in agreement with previous unsuccessful attempts to detect deep level defects induced by LID, we have not observed any SRH states in the DLTS and MCTS spectra recorded after the LID processes induced by forward biasing or light soaking.

However, we have detected rather strong changes in the capacitance of the diodes resulting from the LID processes. Figure 5 shows transients of capacitance (zero shifted by electrical compensation) of a diode from 10 $\Omega \text{ cm}$ Cz-Si:B, which was subjected to forward bias induced degradation (FBID) at 330 K. The transients

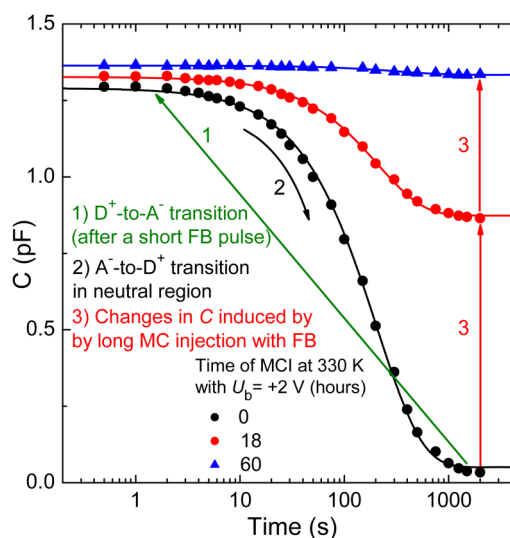


FIG. 5. Capacitance changes upon forward-bias-induced degradation. Changes in compensated diode capacitance $C = C_d - C_b$ at bias voltage $U_b = -10.0 \text{ V}$ and $T = 270 \text{ K}$ after treatments with forward bias (+2 V) induced injection of minority carriers (MCI) at 330 K. The capacitance decays have been initiated by short (10 ms) forward bias pulses and recorded at 270 K upon the application of multiple filling pulses with $U_b = -2.0 \text{ V}$. The solid lines are calculated for a mono-exponential decay process with least-square fitting values of ΔC_m and characteristic decay rate. For the improvement of signal-to-noise ratio in these measurements, we have used a backing-off capacitor of $C_b = 200 \text{ pF}$ to compensate the capacitance of the diode studied (C_d). All the measurements were carried out on an n^+ -p-p⁺ diode from 10 $\Omega \text{ cm}$ p-type Cz-Si:B material which was subjected to a heat treatment at 375 °C for 10 h.

have been induced by short (10 ms) forward bias pulses and recorded at 270 K. The magnitude of the transient is a measure of the H_{390} trap concentration. As shown in Fig. 5, the transformation of the H_{390} trap from the deep donor (state D^+ in Fig. 4) to the shallow acceptor (state A^- in Fig. 4) results in a relatively strong increase in the diode capacitance. Furthermore, a decrease in H_{390} trap concentration (magnitude of the transient) after the FBID process has been observed. The measured data presented in Fig. 5 indicate that the degradation process can be associated with the transformation of the H_{390} trap into another configuration with a shallow acceptor level, which is similar to the configuration A in Fig. 4 but with stronger recombination efficiency.

We have obtained further evidence of the existence of the LID-induced shallow acceptor configuration of the B_sO_2 defect from admittance spectroscopy¹⁵ and low-temperature photoluminescence (PL) measurements. The results of admittance spectroscopy measurements are presented in the [supplementary material](#).

Additional supporting evidence for the generation of a shallow acceptor state during the degradation process and a more incisive insight into its characteristics is provided by low-temperature PL. In these experiments, we have studied samples cut from wafers similar to those used for the 3 Ω cm diode experiments and subjected to degradation by exposure to light of 1 sun intensity from a tungsten-halogen lamp for 60 h at 40 °C. The average lifetime of the BO-degraded material measured by microwave photoconductive decay was 120 μ s, of the as grown material 240 μ s, and of the annealed material 230 μ s. Important changes are observed as a result of the degradation process as shown in Fig. 6. The lower spectrum shown in Fig. 6 is typical of boron-doped Si at 11 K with moderate excitation density. The spectral features are due to excitons bound to the neutral boron acceptor. Although multi-excitonic features are visible, we focus on the boron bound single exciton.

If we compare the LID degraded sample (upper spectrum in Fig. 6) with the annealed sample (lower spectrum), we see the LID results in the appearance of very pronounced shoulders on the peak associated with the boron bound exciton. The energy of the de-convoluted emission in the degraded sample associated with the B_s -related shallow acceptor is 1091.51 meV while the de-convoluted shoulder is at 1092.33 meV, with about half the magnitude of the boron-related peak. The peak position differs from that of the boron bound exciton by 0.82 meV. Using Haynes' rule,²³ this puts the energy level of the acceptor formed during LID at $\sim 45 - (10 \times 0.82 \text{ meV}) \sim 37 \text{ meV}$ from the valence band.

We know from the change in carrier concentration and the DLTS measurement of the H_{390} trap concentration that the concentration of the shallow level giving rise to the 1092.33 meV emission is $\sim 10^{13} \text{ cm}^{-3}$ while the boron concentration is about $4 \times 10^{15} \text{ cm}^{-3}$. Given these very different concentrations, the emission from the exciton bound to the defect associated with the BO degradation is very strong (its intensity is about half that of the boron bound exciton feature). This implies that the oscillator strength of the BO defect is some two orders of magnitude greater than that of boron, which is a surprising result and one that is difficult to reconcile with the defect consisting of a boron atom with an oxygen dimer in the vicinity.

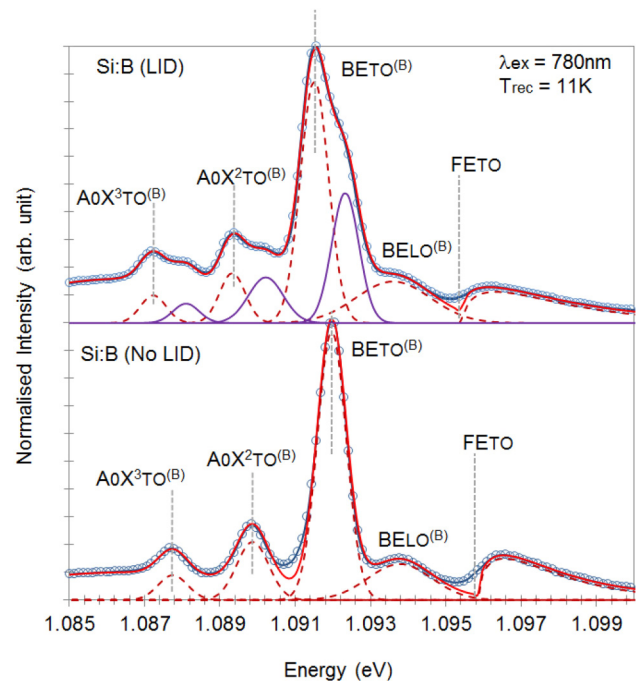


FIG. 6. Low-temperature photoluminescence spectra of 3 Ω cm Cz-Si:B samples before (bottom) and after (top) LID. At 11 K, the bound exciton luminescence dominates. In the spectral region arising from TO phonon replicas, features associated with a single bound exciton and multiple (2 and 3) bound excitons can be observed. The key distinguishing feature in the LID sample is the appearance of a shoulder on the peaks associated with the boron bound exciton (deconvolution of these components shown in purple).

D. LID-induced recombination mechanism: Arguments for occurrence of the trap-assisted Auger recombination

As discussed earlier in this paper, we conclude that SRH is not the dominant recombination mechanism in BO degradation despite the SRH kinetic model being used as a description of the lifetime behavior in several previous publications.

In Fig. 3, we show an inverse relationship between the concentration of the deep precursor donor and the carrier lifetime expressed as a notional recombination center concentration. Furthermore, we show that the deep donor transforms on LID into a shallow acceptor in similar concentrations. Our hypothesis is, therefore, that the shallow acceptor is directly or indirectly responsible for the additional recombination produced by BO degradation. One possibility is that this could occur via a trap Auger process which involves the center with a hole ionization energy of 37 meV observed in PL. This center is responsible for the increase in carrier concentration observed in the transition from the annealed to the degraded state, as detected by CV measurements and admittance spectroscopy.

Trap Auger processes have been studied theoretically but little experimental data exist. Landsberg has published extensively on the theory of this topic, e.g., Ref. 38. Many variants on the trap Auger mechanism are postulated, but in all cases, the Auger recombination

results in an excited “hot” carrier with energy above the bandgap. The detection of such a carrier is, therefore, generally regarded as evidence of an Auger process.

Hangleiter has studied trap Auger processes in silicon doped with transition metals and has detected very weak above bandgap luminescence resulting from the hot carriers emitted as a result of the Auger process.^{25,39} We have undertaken similar experiments comparing annealed and BO-degraded materials and also see very weak above bandgap luminescence as shown in Fig. 7. This work has been done on the same material as used for the low-temperature photoluminescence.

These spectra are noisy but show distinct differences between the degraded and nondegraded samples. The degraded samples show a broad emission with a threshold at about $2\times$ bandgap energy and a peak near 1.85 eV. The nondegraded samples show a slight increase toward longer wavelengths but this is only marginally above the noise. This emission from the degraded material is consistent with Hangleiter’s results but there are some differences. The first and most important is that in our measurements the threshold appears to be close to $2E_g$. In our case, it is difficult to be more precise because of random fluctuations in intensity but we hope to improve this with modifications to the measurement including low-temperature studies. Hangleiter obtained threshold energies of $2E_g - E_T$ where E_T is the Auger trap energy from the majority carrier band. In our case, the shallow acceptor which we believe to be the Auger trap is close to the valence band. In consequence, we expect the threshold to be $2E_g - 37$ meV.

A key difference compared to Hangleiter’s result is the absence of any emission at exactly $2E_g$ due to the phononless simultaneous recombination of two electron hole pairs, which could be due to

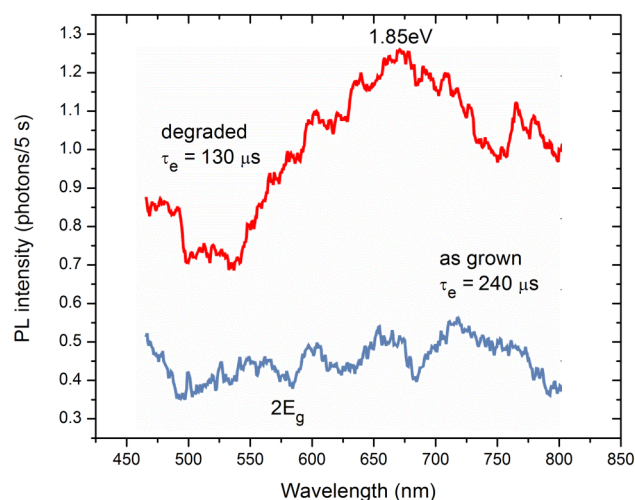


FIG. 7. Above bandgap photoluminescence at 300 K compared for a $3\ \Omega\text{ cm}$ silicon sample in the BO-degraded and annealed states. The spectra are corrected for response of the CCD detector and spectrometer but contain random fluctuations in intensity, making it impracticable to determine an exact threshold for emission in the BO-degraded material (see Sec. II A 5 for experimental details).

the differences in temperatures used. Our measurements were conducted at 300 K, whereas Hangleiter used lower temperatures ~ 70 K.²⁵ At 300 K, the transient exciton population is much less than at 70 K so the probability of a two exciton process is quite small.

In band-to-band Auger recombination, an electron recombines with a hole, giving its energy to a third electron or hole and no impurities or defects are involved, i.e., it is an intrinsic process and for low injection conditions, the minority carrier lifetime depends on the inverse of the square of the carrier concentration. If an impurity is involved in the Auger process, the situation is different and, in principle, the lifetime depends simply on the inverse of the carrier concentration. In the case of the SRH recombination for low injection levels, the lifetime is independent of carrier concentration. So, the overall lifetime, τ , can be expressed as a function of carrier concentration n by

$$1/\tau = \alpha + \beta n + \gamma n^2.$$

This form of relationship has previously been used by Haug⁴⁰ and by Landsberg⁴¹ to fit experimental dependencies of carrier lifetime. Landsberg has shown that inclusion of the second term provides a much improved fit of experimental $\tau(n)$ dependencies at low excitation densities implying that trap Auger may not be uncommon in silicon. In practice, the situation is much more complicated because of Coulomb interaction effects between mobile charge carriers, which, even for the case of band-to-band Auger recombination at low excitation densities, make precise fitting of the lifetime as a function of excitation density quite complex.^{42,43} Furthermore, both the SRH and trap Auger recombination rely on a limited number of defect states so in moderate to high injection regimes the recombination rates of both mechanisms suffer from quasi-saturation of traps with charge carriers, meaning accurate modeling of the recombination process requires knowledge of the occupancy of the defects. This is standard practice for SRH but requires a much greater knowledge of the parameters of the trap Auger process than we currently possess for the boron-oxygen defect. However, it does seem that a lifetime dominated by trap Auger recombination could be credibly parameterized in SRH terms and would display a regime that exhibits an increase in lifetime with increasing excitation density due to saturation of the trap Auger pathway. This was not considered by Landsberg or Haug as they focused on the impact of carrier concentration with low excitation densities.^{40,41}

In 1995, Pang *et al.*⁴⁴ included a trap Auger term in their fitting of solar cell performance and postulated that based on the quality of material available at that time trap Auger was not significant at excitation densities resulting from illumination with 1 sun intensity. Given that more recent works seem to imply that SRH centers have largely been eliminated from high quality material,^{45,46} it is perhaps now more likely that trap Auger recombination, in the form of a BO-related center and/or through other shallow defects, will play a more significant role in the pursuit of further improvements in silicon photovoltaic technology.

IV. AB INITIO MODELING OF B_5O_2 DEFECT

Despite the consensual idea that the BO-degradation defect should include a substitutional boron and a pair of interstitial

oxygen atoms, it is far from clear how these two electrically harmless defects can combine and lead to strong recombination activity. Among the models available in the literature, none are free from conflicts with the observations. For instance, while those involving interstitial boron are unconvincing due to their high formation energy,^{47,48} models possessing substitutional boron require a fast-diffusing and electrically active oxygen dimer (O_2),^{49,50} which as we show below, it is not plausible regardless of the doping conditions.⁵¹

Interstitial O_2 in Si adopts a staggered Si–O–Si–O–Si structure, with two-fold coordinated O atoms being connected to a common Si atom.⁵² This structure is electronically inactive as the oxygen lone-pair states lie deep within the valence band. The oxygen dimer migrates with an activation barrier of 2.0 eV as obtained from annealing kinetics experiments.⁵³ The migration mechanism consists of a concerted hopping of both O atoms toward neighboring bond-center sites. Along the way, the saddle point configuration has two equivalent three-fold coordinated O atoms, forming a four-fold ring structure of Si–O bonds, thus the designation of squared structure. When moving uphill to the transition state, a fully occupied level (made of O lone-pair states) emerges above the valence band top and approaches the conduction band bottom. For that, the squared structure has been claimed to be a double donor, which would be stable in p-type Si. Its migration, allegedly enhanced in the presence of minority carriers, has been a crucial argument in support of the formation kinetics of the LID defect, where recombination-enhanced fast-diffusion of O_2^{++} , combined with Coulomb attraction, would drive the dimers to react with B_s^- dopants.^{49,50}

For neutral O_2 , using the hybrid density functional theory, we estimate a migration barrier of 1.94 eV. While this agrees nicely with the observations, it contrasts with a previous local-density functional barrier of about 1.4 eV.⁵² We explain this discrepancy with the underestimation of the local-density approximated bandgap width in Ref. 52. In those calculations, the donor level of the squared structure over-resonated with the deceptively low conduction band minimum. For that reason, the energy profile along the migration path was effectively cut off at 1.4 eV.

Due to the same effect, the energy of positively charged oxygen dimers was artificially low in Refs. 49 and 50. Additionally, the lack of periodic charge corrections in those works resulted in a further underestimation of energies, particularly for the double plus state, where the correction is almost 0.5 eV. We were able to reproduce the above misleading results and obtain a (0/++) transition at $E_v + 0.15$ eV, but after adding the periodic charge corrections, both (0/+) and (+/++) transitions dropped below the valence band top, meaning that O_2^+ and O_2^{++} are not stable, even in strongly doped Si as recently shown experimentally.⁵¹

The above results refute the idea of a fast-diffusing oxygen dimer species under electron injection conditions. Instead, we suggest that degradation initiates from a B_sO_2 latent state already present in the silicon, which becomes recombination active upon interaction with minority carriers.

In line with previous studies,^{49,50} we found that negatively and positively charged B_sO_2 defects display staggered and squared O_2 units, respectively. Representative “ball-and-stick” models are depicted below the CC diagram of Fig. 8, where O, B, and Si atoms are shown in black, gray, and white, respectively. As detailed below,

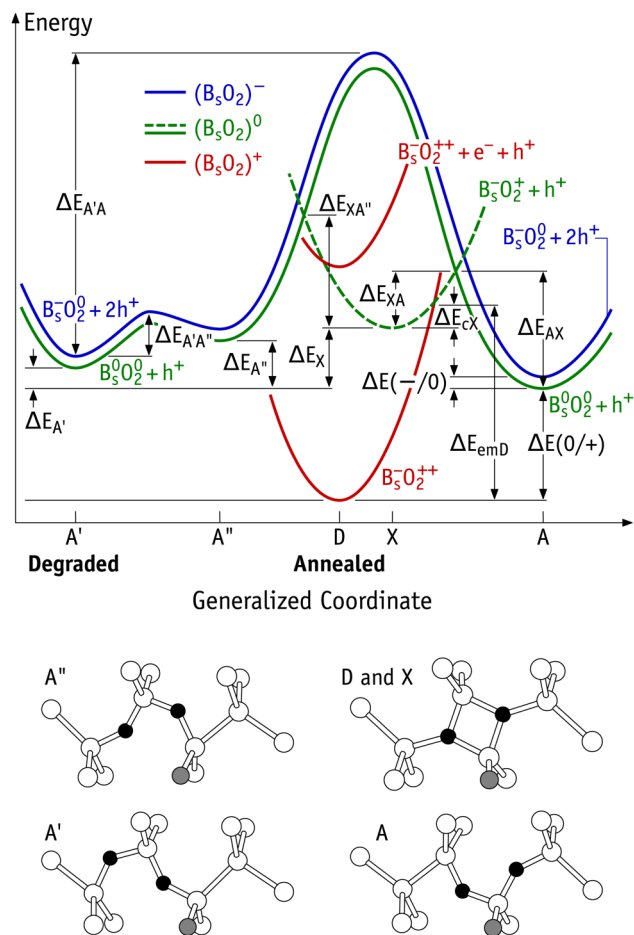


FIG. 8. Configuration coordinate diagram and structures of the B_sO_2 defect. The diagram has been constructed on the basis of first-principles calculations and experimental data presented in Tables I and II. Deep donor squared structures (D and X) as well as shallow acceptor staggered structures (A, A', and A'') are also depicted in the lower part of the figure. According to the model proposed, D and A' structures are assigned to the “Annealed” and “Degraded” states, respectively. See text for further details.

staggered and squared structures show acceptor and donor activity, and as depicted in Fig. 8, they have A-type and {D, X}-type configurations, respectively.

Before continuing, let us briefly address the following question: how can O_2 next to B become a deep donor, while it is electrically inactive when it is far away from the dopant? The answer lies essentially on a prominent strain cancellation involving compressive O atoms and the tensile boron impurity affecting the D structure (when compared to neighboring A-type and separated $O_2 + B_s$ structures). This effect stabilizes the D^+ state against A^0 and it is absent when O_2 and B_s are at remote locations. In that case, configurations O_2^{++} (squared) + B_s^- and O_2^+ (squared) + B_s^0 become unstable as their energy raise above that of O_2^0 (staggered) + B_s^0 .

The electronic structure of $(B_sO_2)^q$ defects in charge state q is rationalized as $B_s^aO_2^d$, with a and d representing the charge of

the B_s -acceptor and O_2 -donor levels (see above), respectively, with $q = a + d$. Structure D is the ground state for $(B_sO_2)^+$, whereas A has the lowest energy for both $(B_sO_2)^0$ and $(B_sO_2)^-$. Neutral A' and A'' are metastable and lie $\Delta E_{A'} = 0.23$ eV and $\Delta E_{A''} = 0.38$ eV above A, respectively. Negatively charged A' and A'' are also metastable with respect to A^- by analogous energy differences. The neutral squared structure is labeled X. The structure is distinguished from D due to a small ~ 0.1 eV Franck-Condon relaxation upon ionization of the deep donor. Neutral X lies $\Delta E_X = 0.56$ eV above neutral A.

The energy difference between D^+ and $X^0 + h^+$ states is calculated as 0.90 eV. Considering that D^+ is a ground state, we assign the $D^+ \rightarrow X^0 + h^+$ transition to the H_{390} hole emission ($\Delta E_{emD} = 0.97$ eV). A-type structures are all shallow acceptors. Small differences in their relative energies simply reveal variable ability to cancel local strain. Their acceptor levels are estimated at $E_v + 0.05$ eV. A meV accurate account of their location is not possible within the present formalism.

Taking the $\Delta E_X = 0.56$ eV difference between X^0 and A^0 , we place the donor level at $E(0/+) = E_v + 0.34$ eV. B_sO_2 is, therefore, a negative- U defect, with the donor level lying considerably above the acceptor level. Accordingly, the thermodynamic $(-/+)$ level is placed at $E(-/+)=E_v+0.20$ eV. Considering the rather different structures involved, the agreement between the above figures and measured $\Delta E(0/+) = 0.56$ eV and $\Delta E(-/+) = 0.3$ eV is rather good.

State A cannot be assigned to the slow-formed recombination defect (SRD). That would be incompatible with the observed transient kinetics involving forward and reverse transitions between D^+ and A^- . Instead, we suggest that state A is responsible for the fast-formed recombination defect (FRD), while A' seems a more plausible contender for SRD. However, such connection must also provide (1) a viable mechanism for the $FRD \rightarrow SRD$ ($A \rightarrow A'$) conversion and (2) an explanation for the actual degradation of free-electron lifetime.

At room temperature, the A structure is ionized in the negative charge state. Along A^- to A'^- , the electronic level occupancy of the defect is $B_s^-O_2^0$, i.e., essentially identical to that of isolated O_2 . The transition state takes place at a structure close to D, and the energy is 1.71 eV above A^- (see blue line in the CC diagram). Such a barrier is simply too high to be surmounted within hours under solar cell operation conditions.

The solid green line in the CC diagram shows the path of the $A^0 \rightarrow A'^0$ transformation in the $B_s^0O_2^0$ state (avoiding a transition to the $B_s^-O_2^+$ electronic state of the X structure). Again, it involves a jump of neutral O_2 , which is now immersed in a diffuse hole (bound to boron). The barrier is, therefore, not expected to differ significantly from 1.7 eV.

Near the X configuration, $B_s^-O_2^+$ is actually the lowest energy neutral state (dashed-green line). We argue that the two-stage mechanism $A^- + h^+ \rightarrow A^0 \rightarrow X^0$ is less probable than simple hole capture $A^- + h^+ \rightarrow X^0$. Whereas the first requires sequential free-to-bound ($B_s^-O_2^0 + h^+ \rightarrow B_s^0O_2^0$) and bound-to-bound ($B_s^0O_2^0$ to $B_s^-O_2^+$) transitions, the second mechanism simply involves a single free-to-bound transition.

We propose that $A \rightarrow A'$ is leveraged by trap Auger recombination of an exciton bound to A^0 . Accordingly, the resulting Auger hole would be promoted to the oxygen lone state, bring the defect

into the $B_s^-O_2^+$ electronic state (dashed-green line), about 1 eV above structure A. Subsequent relaxation along the $B^-O_2^+$ state could drive a jump toward A'^- on the left-hand side of the CC diagram accompanied by hole emission. Importantly, this mechanism involves the capture of two holes (the first due to a free-to-bound capture $A^- + h^+ \rightarrow A^0$, and a second hole as a constituent of an exciton captured by A^0), thus complying with the p^2 dependence of the degradation kinetics. Furthermore, the lifetime recovery of degraded cells under dark annealing is accounted for by the $A' \rightarrow A$ back transformation, with a calculated barrier of $\Delta E_{A'A} = 1.48$ eV. This is close to the measured activation energy of 1.32 eV.^{2,3} The calculated relative energies, transformation barriers, and electrical levels are all summarized in Table II, conferring a quantitative quality to Fig. 8.

We finally report on the thermal stability of B_sO_2 and the effect of involving other p-type dopants. Boron dopants introduce strong tensile strain fields in the Si crystal. These result from (1) a large B/Si size mismatch (the boron atomic radius is about 23% smaller than that of silicon) and (2) comparable Si-Si and B-Si bond strength (about 320 kJ/mol). Since interstitial oxygen complexes (including O_2) are compressive defects, they are prone to stay close to boron. We found that the energy of independent neutral O_2 and B_s^0 (B_s^-) defects is 0.48 eV higher than the A^0 (A^-) state. At temperatures exceeding 350 °C, the Fermi level is close to midgap so that the most probable state of B_sO_2 is A^- . Therefore, assuming that the kinetics of the reaction $(B_sO_2)^- \rightarrow O_2 + B_s^-$ is diffusion-limited by the migration barrier of O_2 , we arrive at a dissociation barrier of about 2.5 eV. These figures explain the annealing behavior of the H_{390} trap—whereas a certain thermal budget ($T > 350$ °C) is needed to increase the concentration H_{390} (enabling the forward reaction via O_2 migration with a barrier of 2 eV), when the temperature exceeds a critical threshold ($T \sim 600$ °C), dissociation of B_sO_2 starts to occur with a 2.5 eV barrier.

It is well known that Ga-doped material does not suffer from light-induced degradation. We calculated the binding energy of

TABLE II. Calculated relative energies of neutral B_sO_2 defects with respect to configuration A, respective transformation barriers, and electrical levels involving ground state structures of neutral, positive, and negative charge states. Symbols are represented in Fig. 8.

Quantity	Calculated value (eV)
Relative energies	
ΔE_X	0.56
$\Delta E_{A'}$	0.23
$\Delta E_{A''}$	0.38
Barriers	
$\Delta E_{A'A''}$	0.20
$\Delta E_{A''A'}$	0.05
$\Delta E_{AA'}$	1.71
$\Delta E_{A'A}$	1.48
Electrical levels	
$\Delta E(0/+) = E(0/+) - E_v$	0.34
$\Delta E(-/0) = E(-/0) - E_v$	0.05
$\Delta E(-/+) = E(-/+) - E_v$	0.20

$\{\text{Al}_s, \text{Ga}_s, \text{In}_s\}\text{O}_2$ complexes (against O_2 plus a remote dopant), and for all of them we find negative values, namely, -0.22 , -0.12 , and -0.17 eV for Al, Ga, and In, respectively. These results consistently follow from the acceptor-Si bond lengths of 2.43, 2.41, and 2.56 Å of isolated Al_s , Ga_s , and In_s , which are all longer than the Si-Si bond in bulk (2.37 Å), effectively producing a compressive strain field. Clearly, all p-type dopants but boron repel O_2 defects.

It should be mentioned that for the case of indium doped silicon there is no consensus regarding experimental results on LID. Möller and Lauer⁵⁴ have reported degradation based on minority carrier lifetime measurements using photo-conductance decay methods, while in an earlier work by Schmidt and Bothe⁵⁵ no degradation has been observed in Al, Ga, or In-doped Si materials. Schmidt and Bothe also used a microwave photoconductive decay technique to measure lifetime but with bias light to minimize the effects of trapping on extraction of lifetime values from the measured decay curves. In a more recent study by Cho *et al.*,⁵⁶ LID effects have been compared in PERC solar cells of ~20% efficiency manufactured from In and B-doped Cz-Si materials. No degradation of the In-doped devices was observed after light soaking (0.8 sun for 48 h) at 37 °C, while the boron doped devices degraded by 0.3–0.5% absolute. At the present time, we have no DLTS results on Si:In samples subjected to LID treatments.

V. RECONCILIATION WITH PREVIOUSLY PUBLISHED RESULTS ON THE BO-RELATED LIFETIME DEGRADATION

We believe that we have obtained solid evidence demonstrating that the BO-related LID is associated with transformations of the BO_2 defect from the configuration with a “squared” oxygen dimer and a substitutional boron atom (a deep donor configuration) to two different configurations with a “staggered” O_2 and B_s (shallow acceptor configurations). The configuration of BO_2 with the “squared” oxygen dimer can be considered the “fully annealed state,” while one of the configurations with the “staggered” O_2 close to B_s produces the degraded state.

How our model is consistent with previously observed characteristic features of the BO-related LID?

Before comparing the specific LID-related results from the literature with those obtained by us, we would like to mention the following. Our findings indicate that some results reported in the literature on the BO LID problem in Si (both p- and n-types) must be considered with great care because of the limitations of the lifetime measurements technique used. The majority of results on BO LID in Si have been collected from quasi-steady-state photo-conductance (QSS-PC) measurements with the use of a simplified approach which does not take into account effects of carrier trapping by the BO LID defect precursor in p-type Si and by bistable oxygen-related thermal double donors (BTDDs) in compensated n-type Si. The transformation of the B_sO_2 defect from the D^+ state to the A^- state (Figs. 4 and 5) in nondegraded or partially degraded p-type Si upon illumination results in significant persistent photo-conductivity. Often this is not taken into account when calculating minority carrier lifetime although the effects of trapping in QSS-PC are well documented in the literature.^{57–59} The BTDD defects, which are formed simultaneously with the B_sO_2 defect, are responsible for

the appearance of this persistent photo-conductivity in oxygen-rich n-type Cz-Si samples.^{60–62} So, the simplified analysis of QSS-PC measurements in both p- and n-type Si crystals with the B_sO_2 defect can result (and have resulted) in significant errors in determination of lifetime values and further in calculations of relative concentrations and recombination parameters of the B_sO_2 defect.

- (i) Dependencies of concentration the BO defect responsible for LID on oxygen and boron concentrations and formation and annealing conditions of the defect.^{2,3,34–37,55}

As it has already been mentioned, as yet, we do not have a set of Si samples with different and precisely measured oxygen and boron concentrations to obtain proper dependencies of the H_{390} trap concentration on $[\text{O}_i]$ and $[\text{B}_s]$. However, our B_sO_2 model is consistent with the reported dependencies of the BO defect responsible for LID on $[\text{O}_i]$ and $[\text{B}_s]$ and the results obtained shed some new light on the formation and annealing conditions of the center. The $[\text{O}_i]$ and $[\text{B}_s]$ dependencies have been obtained on samples from as-grown boron-doped Cz-Si crystals.^{2,3} It has been shown that the concentration of the oxygen dimer in as-grown Cz-Si samples is nearly proportional to the squared concentration of interstitial oxygen atoms.⁵¹ So, the interaction of mobile oxygen dimers with B_s atoms at temperatures exceeding 350 °C explains the observed concentration dependencies. We have found that the B_sO_2 complex can be formed upon heat treatments in the temperature range 350–450 °C where the oxygen dimer is mobile; however, the binding energy of the complex is not very high, so heat treatments at higher temperatures ($T \geq 600$ °C) result in its dissociation and the reduced LID extent.^{2,35–37}

- (ii) Kinetics of the BO-related LID and p^2 dependence of the degradation rate.^{2,3,55}

Our data on the transformation kinetics of the BO_2 defect upon minority carrier injection are consistent with the previously published results on the BO-related LID. Furthermore, our measurements on the diodes from 3 and 10 Ω cm Cz-Si:B materials indicate a p^2 dependence of the rate of disappearance of the H_{390} trap upon minority carrier injection treatments. We suggest that the p^2 dependence of the BO-related LID can be explained by the recombination induced transition from one shallow acceptor state of the B_sO_2 defect to another shallow acceptor configuration with higher recombination activity. Such a transition consists of the capture of a hole and a charge state change from single negative to neutral with subsequent capture of an exciton and its recombination. This releases enough energy for surmounting the energy barrier for configuration transformation. So, the capture of two holes is necessary to promote the transformation.

- (iii) Electronic characteristics of the defect responsible for the BO-related LID.^{2,10–13,55,63,64}

Our results are not consistent with the previous suggestions that the defect responsible for the “fast” and “slow” BO LID is related to recombination active centers with deep donor levels that are close to Si midgap although in several cases SRH kinetic equations have been used to fit BO LID data.^{10–13,55} As it has been already mentioned, such centers can be relatively easily detected in MCTS

measurements on *p*-type Cz-Si crystals. The DLTS/MCTS signals due to deep traps, which were linked with the BO recombination centers, were reported in one paper;¹⁶ however, the results have not been reproduced in further studies. We argue that the BO LID is related to the trap-assisted Auger recombination through the BO₂ defect in a shallow acceptor configuration. For some reasons, which are not fully understood yet, the recombination activity of BO₂ in this configuration is much stronger than the recombination activity of substitutional boron atoms.

(iv) “Fast” and “slow” BO-related LID.^{2–4,55,63–65}

We have not studied carefully the “fast” BO LID. It can be speculated that the “fast” BO LID is related to the rapid transformation of the BO₂ defect from the configuration with the deep donor state to the shallow acceptor state A (Fig. 8). Our measurements indicate that the energy barrier for this process $\Delta E_{XA} \lesssim 0.26$ eV (Fig. 3 and Table I), which is in line with an activation energy of 0.23 eV for “fast” LID reported in Ref. 3. However, other origins of the “fast” LID are possible.

We suggest that the “slow” LID is related to the transition of the BO₂ defect from the A state to the A' state through the metastable X state. This process involves surmounting the higher energy barrier $\Delta E_{XA'}$ depicted in Fig. 8 (the energy barrier for the “slow” LID is ~ 0.45 eV according to Ref. 3). We argue that the A \rightarrow A' process is promoted by an Auger-recombination event when the defect is in state A.

Importantly, the diffuse shallow acceptor state of boron and the oxygen-related states are essentially the same for both A and A' configurations. Hence, both these configurations are suggested to have almost identical trap Auger recombination activity. This can explain the similar recombination parameters obtained in Refs. 4 and 13 for the “fast” and “slow” LID defects. The observations in Refs. 4 and 13 were interpreted as an indication of a single recombination active LID defect, which is not consistent with our view.

(v) Lifetime recovery after long- and short-term dark anneals.^{2–4}

The recovery of lifetime after long-term dark anneals is thought to reflect the return of the B₃O₂ defect from the A' degraded state to the ground D⁺ state (Fig. 8). According to Fig. 8, this could proceed by first jumping over the energy barrier $\Delta E_{A'A}$ into the A state, which was calculated as $\Delta E_{A'A} = 1.48$ eV. This value compares well with the measured energy barrier of 1.32 eV for the recovery from the “slow” LID.^{2,3} However, we must consider that other possibilities could apply as well.

We are currently investigating an explanation for the prevailing “fast” degradation observed in Ref. 4 after short dark anneals (e.g., 170 °C for about 1 min) of fully degraded samples.

(vi) Stabilized BO LID state.^{2,7,9,66}

We have not been able to transform the degraded BO-related state into the stabilized form in the diodes studied. It is now generally accepted that hydrogen plays a role in the formation of the stabilized state. Our diode structures have been designed to try to eliminate hydrogen from the active region and we have not detected any signs of hydrogen in our *n*⁺-*p*-*p*⁺ diodes which, in general, would

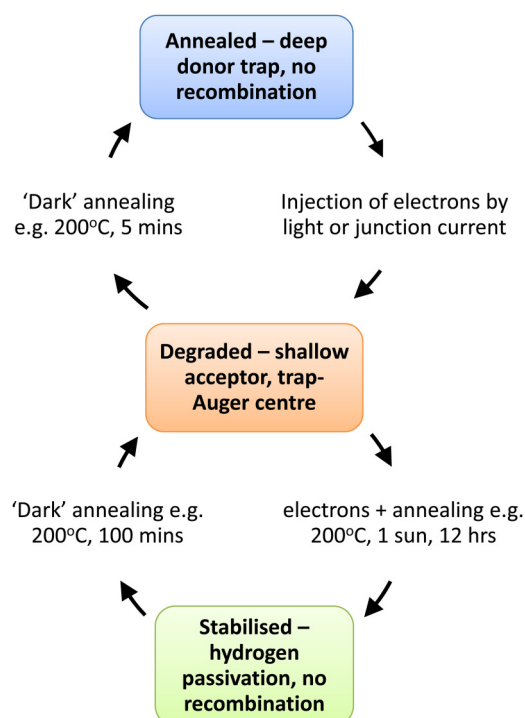


FIG. 9. Block diagram of the BO LID-related defect states and processes. Overview of the ground and two metastable states of the BO-related defect with identities fitting the experimental and theoretical results in this publication. The atomic structures of the defects are presented together with the configuration coordinate diagram in Fig. 8.

be apparent as weak bonding of the hydrogen to some of the boron and subsequent carrier reduction. Our results, therefore, provide support for the hypothesis of hydrogen being necessary for the formation of the stabilized state.

VI. CONCLUSIONS

We have shown that in *n*⁺-*p*-*p*⁺ diodes fabricated from boron-doped Cz silicon, in a way that minimizes the presence of hydrogen in the active region, a defect with negative-*U* properties exists, which is related to the oxygen content and thermal treatment of the silicon. On minority carrier injection, this defect is transformed into a shallow acceptor. This is evident in terms of increased carrier concentration, in admittance spectroscopy and in low-temperature photoluminescence. The unusual characteristics of the negative-*U* defect and its transformation into a shallow acceptor are explained by the configuration coordinate diagram shown in Fig. 8.

The minority carrier lifetime of the silicon decreases as the concentration of the negative-*U* defect decreases. Dark annealing restores the original concentration of the defect with *U* < 0 and eliminates the shallow acceptor which was formed from it. The thermal and electron injection conditions match those widely

reported for the transitions between the annealed and the degraded states associated with BO degradation. Although we have not yet extended these results to a range of oxygen and boron concentrations (something we intend to do in the near future), the match of the conditions (temperatures and times) of transition between annealed and degraded states in our experiments and those reported for the BO-degradation process is strong evidence for the involvement of the defects we have characterized in the BO degradation.

Ab initio calculations have been able to suggest atomic structures of the defect states and a configuration coordinate diagram very similar to those determined experimentally from the DLTS measurements. In line with previous studies, we found that the most stable configurations of the B_5O_2 defect are charge state dependent. Negatively and positively charged states adopt staggered and squared forms of the oxygen dimer while counteracting strain between the dimer and boron has a significant effect on the defect properties. The proposed stable atomic configurations of the B_5O_2 defect are shown in the lower part of Fig. 8, and a summary of how the findings of defect properties and structure reported in this paper relate to the known LID phenomena is given in Fig. 9.

Considering the low concentrations of the B_5O_2 -related shallow acceptor defect, its impact on the bound exciton luminescence is surprisingly large, implying an oscillator strength two orders of magnitude greater than that of boron. The preliminary observation of above bandgap luminescence with a threshold energy around $2E_g$ in the degraded material suggests a trap Auger effect involving the shallow acceptor. Again, this is an issue requiring more work in terms of both refining the measurements of hot electron emission and understanding how such a process can occur with such a shallow acceptor.

SUPPLEMENTARY MATERIAL

See the [supplementary material](#) for more detailed experimental results on electronic and recombination properties of the precursor of the boron–oxygen LID defect and on admittance spectroscopy of shallow acceptors in annealed degraded boron-doped Cz-Si samples.

ACKNOWLEDGMENTS

The project was funded by the UK EPSRC under Contract No. EP/M024911/1. This joint project between Warwick, Manchester, and Oxford Universities was co-ordinated by John Murphy; we would like to thank him and all the other contract participants for discussions on solar silicon. M.V.-C. would like to thank CONACyT-Mexico for financial support. J.C. thanks the Fundação para a Ciência e a Tecnologia (FCT) for support under Contract No. UID/CTM/50025/2013, co-funded by FEDER funds through the COMPETE 2020 Program. We are extremely grateful to Bob Falster and Vladimir Voronkov of SunEdison Semiconductor for important discussions and the supply of carefully selected silicon slices and to Chris Van de Walle, Claude Weisbuch, and Jim Speck of UCSB for discussions on Auger processes. We thank Brett Hallam for discussions and access to UNSW data prior to publication. We would like to thank Simon Hammersley for assistance with the measurements and Mal McGowan for clean room facilities.

REFERENCES

- 1M. A. Green, *Nat. Energy* **1**, 15015 (2016).
- 2T. Niewelt, J. Schön, W. Warta, S. W. Glunz, and M. C. Schubert, *IEEE J. Photovolt.* **7**, 383 (2017).
- 3K. Bothe and J. Schmidt, *J. Appl. Phys.* **99**, 013701 (2006).
- 4M. Kim, M. Abbott, N. Nampalli, S. Wenham, B. Stefani, and B. Hallam, *J. Appl. Phys.* **121**, 053106 (2017).
- 5K. Bothe, R. Hezel, and J. Schmidt, *Appl. Phys. Lett.* **83**, 1225 (2003).
- 6J. Lindroos and H. Savin, *Solar Energy Mater. Solar Cells* **147**, 115 (2016).
- 7A. Herguth and G. Hahn, *J. Appl. Phys.* **108**, 114509 (2010).
- 8K. Arafune, T. Sasaki, F. Wakabayashi, Y. Terada, Y. Ohshita, and Y. Yamaguchi, *Physica B* **376–377**, 236 (2006).
- 9B. Hallam, A. Herguth, P. Hamer, N. Nampalli, S. Wilking, M. Abbott, S. Wenham, and G. Hahn, *Appl. Sci.* **8**, 10 (2018).
- 10J. Schmidt and A. Cuevas, *J. Appl. Phys.* **86**, 3175 (1999).
- 11S. Rein and S. W. Glunz, *Appl. Phys. Lett.* **82**, 1054 (2003).
- 12T. Niewelt, J. Schön, J. Broisch, W. Warta, and M. Schubert, *Phys. Status Solidi RRL* **9**, 692 (2015).
- 13B. Hallam, M. Abbott, T. Nærland, and S. Wenham, *Phys. Status Solidi RRL* **10**, 520 (2016).
- 14R. Brunwin, B. Hamilton, P. Jordan, and A. R. Peaker, *Electron. Lett.* **15**, 349 (1979).
- 15A. R. Peaker, V. P. Markevich, and J. Coutinho, *J. Appl. Phys.* **123**, 161559 (2018).
- 16T. Mchedlize and J. Weber, *Phys. Status Solidi RRL* **9**, 108 (2015).
- 17J. Mullins, S. Leonard, V. P. Markevich, I. D. Hawkins, P. Santos, J. Coutinho, A. G. Marinopoulos, J. D. Murphy, M. P. Halsall, and A. R. Peaker, *Phys. Status Solidi A* **214**, 1700304 (2017).
- 18B. Hallam, M. Abbott, N. Nampalli, P. Hamer, and S. Wenham, *J. Appl. Phys.* **119**, 065701 (2016).
- 19V. P. Markevich and L. I. Murin, *Fiz. Tech. Poluprovodn. (S.-Peterburg)* **22**, 911 (1988) [*Sov. Phys. Semicond.* **22**, 574 (1988)].
- 20L. F. Makarenko, M. Moll, F. P. Korshunov, and S. B. Lastovski, *J. Appl. Phys.* **101**, 113537 (2007).
- 21L. Dobaczewski, A. R. Peaker, and K. Bonde Nielsen, *J. Appl. Phys.* **96**, 4689 (2004).
- 22H. J. Kuno, *IEEE Trans. Electron Devices* **11**, 8 (1964).
- 23J. R. Haynes, *Phys. Rev. Lett.* **4**, 361 (1960).
- 24M. P. Halsall, I. F. Crowe, J. Mullins, R. A. Oliver, M. J. Kappers, and C. J. Humphreys, *ACS Photonics* **5**, 4437 (2018).
- 25A. Hangleiter, *Phys. Rev. B* **35**, 9149 (1987).
- 26P. E. Blöchl, *Phys. Rev. B* **50**, 17953 (1994).
- 27G. Kresse and J. Furthmüller, *Phys. Rev. B* **54**, 11169 (1996).
- 28J. P. Perdew, K. Burke, and M. Ernzerhof, *Phys. Rev. Lett.* **77**, 3865 (1996).
- 29J. Heyd, G. E. Scuseria, and M. Ernzerhof, *J. Chem. Phys.* **118**, 8207 (2003).
- 30H. J. Monkhorst and J. D. Pack, *Phys. Rev. B* **13**, 5188 (1976).
- 31G. Makov and M. C. Payne, *Phys. Rev. B* **51**, 4014 (1995).
- 32C. Freysoldt, J. Neugebauer, and C. G. Van de Walle, *Phys. Rev. Lett.* **102**, 016402 (2009).
- 33G. Henkelman and H. Jónsson, *J. Chem. Phys.* **113**, 9901 (2000).
- 34M. Forster, E. Fourmond, F. E. Rougieux, A. Cuevas, R. Gotoh, K. Fujiwara, S. Uda, and M. Lemiti, *Appl. Phys. Lett.* **100**, 042110 (2012).
- 35S. W. Glunz, S. Rein, J. Y. Lee, and W. Warta, *J. Appl. Phys.* **90**, 2397 (2001).
- 36J. Y. Lee, S. Peters, S. Rein, and S. W. Glunz, *Progr. Photovolt. Res. Appl.* **9**, 417 (2001).
- 37D. C. Walter, B. Lim, K. Bothe, V. V. Voronkov, R. Falster, and J. Schmidt, *Appl. Phys. Lett.* **104**, 042111 (2014).
- 38P. T. Landsberg and D. J. Robbins, *Solid State Electron.* **21**, 1289 (1978).
- 39A. Hangleiter, *Phys. Rev. Lett.* **55**, 2976 (1985).
- 40A. Haug, *Phys. Status Solidi B* **108**, 443 (1981).
- 41P. T. Landsberg, *Appl. Phys. Lett.* **50**, 745 (1987).
- 42A. Hangleiter and R. Hacker, *Phys. Rev. Lett.* **65**, 215 (1990).

- ⁴³P. P. Altermatt, J. Schmidt, G. Heiserm, and A. G. Aberle, *J. Appl. Phys.* **82**, 4938 (1997).
- ⁴⁴S. K. Pang, A. W. Smith, and A. Rohatgi, *IEEE Trans. Electron Devices* **42**, 662 (1995).
- ⁴⁵T. Niewelt, A. Richter, T. C. Kho, N. E. Grant, R. S. Bonilla, B. Steinhäuser, J.-I. Polzin, F. Feldmann, M. Hermle, J. D. Murphy, S. P. Phang, W. Kwapil, and M. C. Schubert, *Solar Energy Mater. Solar Cells* **185**, 252 (2018).
- ⁴⁶B. A. Veith-Wolf, S. Schafer, R. Brendel, and J. Schmidt, *Solar Energy Mater. Solar Cells* **186**, 194 (2018).
- ⁴⁷A. Carvalho, P. Santos, J. Coutinho, R. Jones, M. J. Rayson, and P. R. Briddon, *Phys. Status Solidi A* **209**, 1894 (2012).
- ⁴⁸X. Chen, X. Yu, X. Zhu, P. Chen, and D. Yang, *Appl. Phys. Express* **6**, 041301 (2013).
- ⁴⁹J. Adey, R. Jones, D. W. Palmer, P. R. Briddon, and S. Öberg, *Phys. Rev. Lett.* **93**, 055504 (2004).
- ⁵⁰M.-H. Du, H. M. Branz, R. S. Crandall, and S. B. Zhang, *Phys. Rev. Lett.* **97**, 256602 (2006).
- ⁵¹L. I. Murin, E. A. Tolkacheva, V. P. Markevich, A. R. Peaker, B. Hamilton, E. Monakhov, B. G. Svensson, J. L. Lindström, P. Santos, J. Coutinho, and A. Carvalho, *Appl. Phys. Lett.* **98**, 182101 (2011).
- ⁵²J. Coutinho, R. Jones, P. R. Briddon, and S. Öberg, *Phys. Rev. B* **62**, 10824 (2000).
- ⁵³V. Quemener, B. Raciassi, F. Herklotz, L. I. Murin, E. V. Monakhov, and B. G. Svensson, *J. Appl. Phys.* **118**, 135703 (2015).
- ⁵⁴C. Möller and K. Lauer, *Phys. Status Solidi RRL* **7**, 461 (2013).
- ⁵⁵J. Schmidt and K. Bothe, *Phys. Rev. B* **69**, 024107 (2004).
- ⁵⁶E. Cho, Y.-W. Ok, A. D. Upadhyaya, M. J. Binns, J. Appel, J. Guo, and A. Rohatgi, *IEEE J. Photovolt.* **6**, 795 (2016).
- ⁵⁷D. Macdonald, R. A. Sinton, and A. Cuevas, *J. Appl. Phys.* **89**, 2772 (2001).
- ⁵⁸J. Schmidt, K. Bothe, and R. Hezel, *Appl. Phys. Lett.* **80**, 4395 (2002).
- ⁵⁹R. A. Bardos, T. Trupke, M. C. Schubert, and T. Roth, *Appl. Phys. Lett.* **88**, 053504 (2006).
- ⁶⁰V. D. Tkachev, L. F. Makarenko, V. P. Markevich, and L. I. Murin, *Sov. Phys. Semicond.* **18**, 324 (1984).
- ⁶¹Y. Hu, H. Schön, E. J. Øvrelid, Ø. Nielsen, and L. Arnberg, *J. Appl. Phys.* **111**, 053101 (2012).
- ⁶²V. P. Markevich, M. Vaqueiro-Contreras, S. B. Lastovskii, L. I. Murin, M. P. Halsall, and A. R. Peaker, *J. Appl. Phys.* **124**, 225703 (2018).
- ⁶³K. Bothe and J. Schmidt, *Appl. Phys. Lett.* **87**, 262108 (2005).
- ⁶⁴V. V. Voronkov, R. Falster, K. Bothe, B. Lim, and J. Schmidt, *J. Appl. Phys.* **110**, 063515 (2011).
- ⁶⁵M. Kim, D. Chen, M. Abbott, N. Nampalli, S. Wenham, B. Stefani, and B. Hallam, *J. Appl. Phys.* **123**, 161586 (2018).
- ⁶⁶S. Wilking, A. Herguth, and G. Hahn, *J. Appl. Phys.* **113**, 194 (2013).